Vol. 48 (2017) ACTA PHYSICA POLONICA B No 6

PRODUCTION MEASUREMENTS AT THE LHCb*

Bartłomiej Rachwał

on behalf of the LHCb Collaboration

AGH-UST University of Science and Technology, Kraków, Poland

(Received April 10, 2017)

Version corrected according to Erratum Acta Phys. Pol. B **49**, 197 (2018)

The LHCb detector, with its excellent momentum resolution and flexible trigger strategy, is ideally suited for measuring heavy-quark and quarkonia production properties. In addition, the new system of forward shower counters installed upstream and downstream has begun to be used, therefore the experiment is being suited to measure central exclusive production. The LHCb measurements of inclusive and differential cross sections of the production of J/ψ resonance and J/ψ pairs, as well as bottom quarks and Z^0 boson, based on Run 2 datasets are summarized. Finally, results on the prompt production of open charm hadrons and the exclusive production of charmonium are discussed.

DOI:10.5506/APhysPolB.48.1157

1. Introduction

The detailed studies of heavy-flavour production and the comparison to predictions yield an important testing ground for both perturbative and non-perturbative aspects of Quantum Chromodynamics (pQCD, QCD) calculations for high-energy collisions. It is a far-reaching issue of testing models and provide an input to tune simulation. The dominant uncertainties for the theoretical predictions originate from higher order contributions.

From experimental perspectives, the uncertainty in the knowledge of the heavy-quark production cross section limits the sensitivity to searches for physics beyond the Standard Model (SM). As an example, decays of hadrons containing a b quark are often dominant background processes.

The Central Exclusive Production (CEP) in pp collisions is a diffractive process in which the protons remain intact and the meson is produced through the fusion of a photon and a colourless strongly-coupled object, the

* Presented at the Cracow Epiphany Conference "Particle Theory Meets the First Data from LHC Run 2", Kraków, Poland, January 9–12, 2017.

so-called Pomeron. From the experimental point of view, it is a very clean environment of final states. It allows searches for exotic states in a low-background experimental environment and probes the gluon distribution of the proton.

2. LHCb detector and Run 2 data

The LHCb detector [1] is a single-arm forward spectrometer, fully instrumented in the pseudorapidity range $2 < \eta < 5$. The detector includes a high-precision tracking system consisting of a silicon-strip vertex detector (VELO) surrounding the pp interaction region and tracking stations in front and behind of the dipole magnet.

The LHCb datasets of pp collisions recorded at different centre-of-mass energies are shown in Fig. 1. The data used in the analyses presented in this proceedings comes from Run 2 data taking period of 2015 and 2016. These data samples correspond to an integrated luminosity of 0.32 and 1.67 fb^{-1}, respectively.

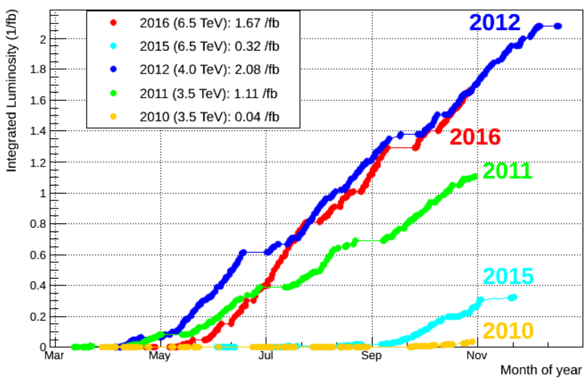

Fig. 1. The LHCb datasets accumulated over Run 1 and 2 data taking periods (from [2]).

To increase the pseudorapidity coverage of the LHCb spectrometer, forward shower counters consisting of five planes of scintillators (HeRSCheL) at −114, −19.7, −7.5, +20 and +114 m from the interaction point have been installed for Run 2, which started in 2015. The combination of VELO and HeRSCheL has sensitivity to particles in the regions of $-10 < \eta < -5$, $-3.5 < \eta < -1.5$, $1.5 < \eta < 10$.

3. Heavy-quark production

3.1. Open charm: D^0, D_s, D^+, D^{*+}

Open charm production at the LHCb is dominated by gluon–gluon scattering, hence the results have a sensitivity to the gluon distribution in the proton at high and low x (down to 10^{-4}) [3].

In pp collisions, charmed mesons can be produced directly from hard collisions of partons, through the feed-down of excited states, or via decays of b-flavoured hadrons. The first two sources are referred to as prompt production, while the third one (secondary charm) is referred to as from-b. For this analysis, the latter is considered as a background.

Double differential cross-sections measurements for the prompt production of D^0, D_s, D^+ and D^{*+} mesons at the LHCb for Run 2 data have been performed for 13 TeV [4] with respect to transverse momentum, p_{T}, and pseudorapidity, η, of the charmed meson. The phase space of the measurement yielded for $2.0 < \eta < 4.5$ and $0 < p_{\mathrm{T}} < 15$ GeV$/c$. This measurement is complementary to the previous one performed at lower energies of $\sqrt{s} = 5$ [5] and 7 TeV [6].

The total $c\bar{c}$ production cross section, $\sigma(pp \to c\bar{c}X)$, has been calculated using the fragmentation fractions from e^+e^- colliders. For the combination of the D^0 and D^+ measurements, one obtained

$$\sigma(pp \to c\bar{c}X) = 2840 \pm 3\ (\mathrm{stat.}) \pm 170\ (\mathrm{syst.}) \pm 150\ (\mathrm{frag.})\ \mu\mathrm{b}\,, \tag{1}$$

where the third error is related to fragmentation fraction.

The LHCb results have been compared with the predictions of charm meson cross sections which are available in pQCD at next-to-leading order (NLO) using the general-mass variable-flavour-number scheme (GMVFNS) [7] and at fixed order with next-to-leading-log resummation (FONLL) [8].

Figure 2 shows one of those comparisons, where the double differential prompt D^0 cross section at $\sqrt{s} = 13$ TeV [4] is plotted. Predictions show large uncertainties at low p_{T} and the data tends to lie at the upper end. However, the individual cross sections are described by the predictions reasonably well.

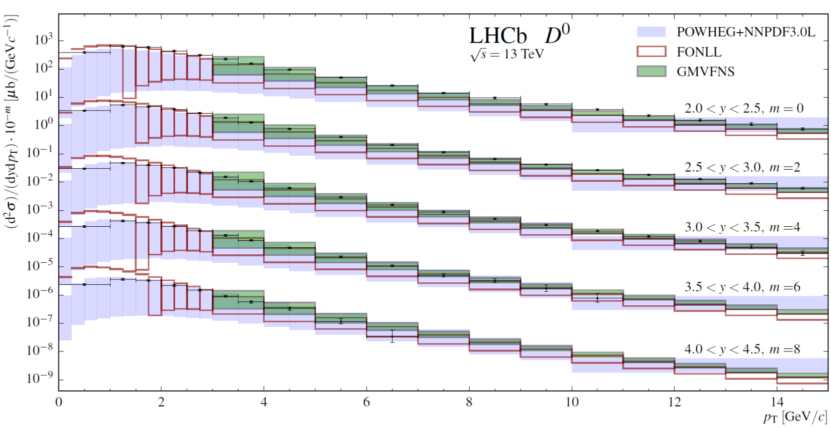

Fig. 2. Measurements and predictions for the double differential prompt D^0 cross section at $\sqrt{s} = 13$ TeV (from [4]).

Figure 3 shows the ratio of the cross sections between $\sqrt{s} = 13$ and 5 TeV [5] and an integrated cross sections compared to the theory predictions.

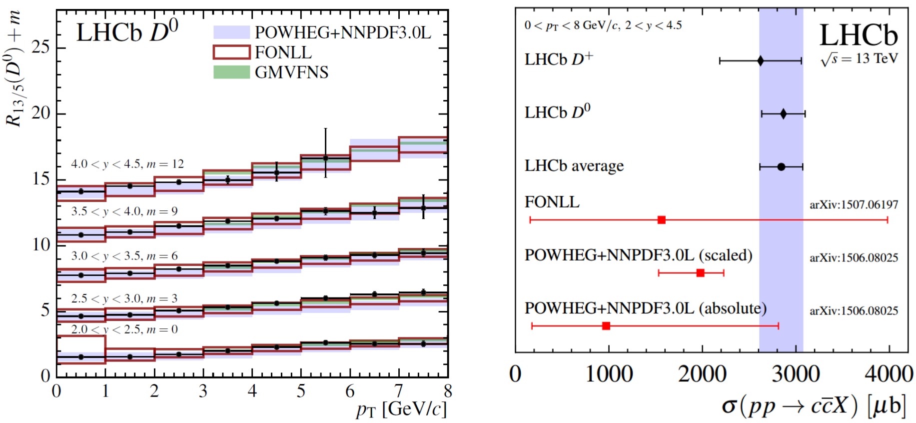

Fig. 3. The prompt D^0 cross-section ratios between $\sqrt{s} = 13$ and 5 TeV (from [5]) (left) and an integrated cross sections (right) compared to the theory predictions (from [4]). The individual datapoints are labelled in the legend, where the *scaled* predictions are based on calculations of the 13 to 7 TeV ratio multiplied with the LHCb results at 7 TeV, while absolute value is based on calculations of the 13 TeV cross section.

3.2. Bottom

The production cross sections for the average of b flavoured and $\bar{b}$ flavoured is measured using semileptonic decays of b hadrons to charm hadrons (D^0, D^+, D_s, Λ_c), where the vertex formed by the muon and the charm hadron is detached from the PV [9]. For the signal extraction, the simultaneous fit to invariant mass and logarithm of impact parameter distributions has been performed. The latter discriminant allows to separate prompt charm-from charm-from b-hadron, where the prompt production of charm hadrons is treated as a background.

The integrated cross sections in the covered η range are:

$$\sigma(pp \to H_b X) = 72.0 \pm 0.3\,(\text{stat.}) \pm 6.8\,(\text{syst.})\ \mu\text{b}\,, \tag{2}$$

$$\sigma(pp \to H_b X) = 154.3 \pm 1.5\,(\text{stat.}) \pm 14.3\,(\text{syst.})\ \mu\text{b} \tag{3}$$

for 7 and 13 TeV. The ratio is found to be $2.14 \pm 0.02 \pm 0.13$, where the quoted uncertainties are statistical and systematic, respectively.

Figure 4 shows the differential cross section as a function of η for $\sigma(pp \to H_b X)$, where H_b is a hadron that contains either a b or a $\bar{b}$ quark, at $\sqrt{s} =$ 7 TeV and 13 TeV superimposed with the predictions from the FONLL [8]. The predictions describe the measurement at both centre-of-mass energies within uncertainties.

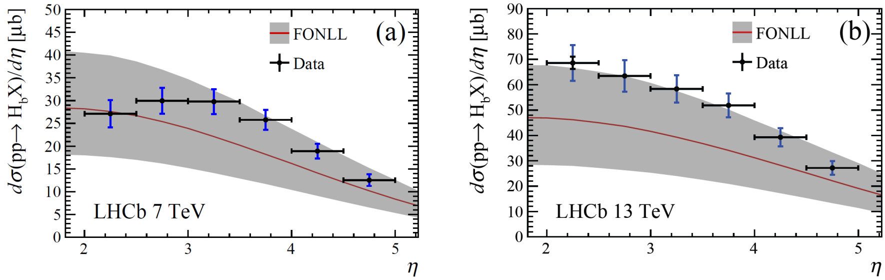

Fig. 4. Differential cross section as a function of η for $(pp \to H_b X)$, where H_b is a hadron that contains either a b or a $\bar{b}$ quark, (a): $\sqrt{s} = 7$ TeV and (b): 13 TeV (from [9]). The measurements are compared to the predictions from FONLL.

4. Quarkonia production

4.1. J/ψ production

The J/ψ cross-section measurement in pp collisions at $\sqrt{s} = 13$ TeV performed at the LHCb benefits from a new scheme for the software trigger introduced at the LHCb for LHC Run 2 [10]. The analysis uses the on-line reconstruction for the first time at the LHCb.

J/ψ mesons are reconstructed in the dimuon final state with p_{T} of the dimuon system restricted to $p_{\mathrm{T}} < 14$ GeV/c and $2.0 < \eta < 4.5$. The excellent vertexing capability of LHCb allows a separation of prompt mesons and J/ψ-from-b [11].

For the signal extraction, a combined fit to the dimuon invariant mass and the pseudo-proper time distribution has been performed. The latter is defined as

$$t_z = \frac{(z_{J/\psi} - z_{\mathrm{PV}})\, M_{J/\psi}}{p_z}\,, \tag{4}$$

where $z_{J/\psi}$ is the position of the J/ψ decay vertex, z_{PV} that of the primary vertex, p_z the z component of the measured J/ψ momentum, and $M_{J/\psi}$ is the reconstructed mass of the J/ψ candidate.

The production cross sections integrated over the kinematic coverage is found to be

$$\sigma(J/\psi_{\mathrm{prompt}}) = 15.30 \pm 0.03\,(\mathrm{stat.}) \pm 0.86\,(\mathrm{syst.})\ \mu\mathrm{b}\,, \tag{5}$$
$$\sigma(J/\psi_{\mathrm{from}\ b-\mathrm{hadron}}) = 2.34 \pm 0.01\,(\mathrm{stat.}) \pm 0.13\,(\mathrm{syst.})\ \mu\mathrm{b}\,. \tag{6}$$

The cross section obtained for J/ψ mesons from b-hadron decays is used to extrapolate to a total $b\bar{b}$ production cross section, which is found to be

$$\sigma(pp \to b\bar{b}X) = 515 \pm\ 2(\mathrm{stat.}) \pm 53\,(\mathrm{syst.})\ \mu\mathrm{b}\,. \tag{7}$$

Figure 5 shows the single differential production cross sections for prompt J/ψ and J/ψ-from-b as a function of $p_{\rm T}$ in the forward region at $\sqrt{s} =$ 13 TeV. The results are superimposed with the non-relativistic QCD (NRQCD) [12] for prompt J/ψ and FONLL for J/ψ-from-b. The cross section for J/ψ-from-b is about a factor of ten smaller than for prompt J/ψ with a $p_{\rm T}$ and η dependence similar to what was observed by the LHCb at lower $\sqrt{s}$.

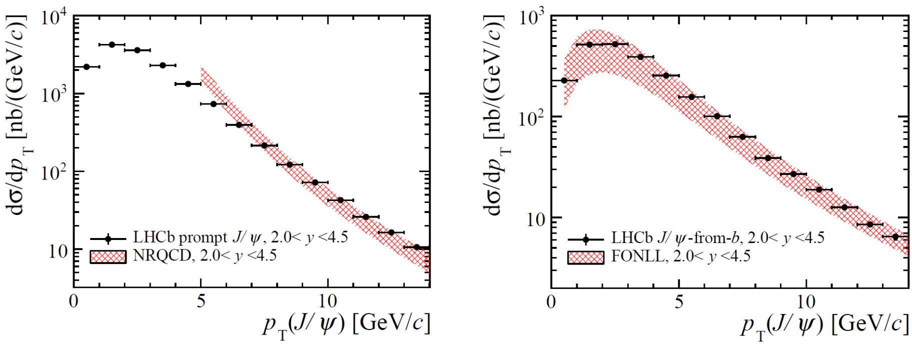

Fig. 5. Differential cross sections as a function of $p_{\rm T}$, (left) compared with the nonrelativistic QCD (NRQCD) calculation for prompt J/ψ and (right) with the FONLL calculation for J/ψ-from-b meson (from [11]).

4.2. J/ψ pairs production

The J/ψ pairs production measurement is based on data collected in 2015 [13]. It is performed for J/ψ mesons with a transverse momentum of less than 10 GeV/c in the rapidity range of $2.0 < y < 4.5$ of the LHCb acceptance, where the polarisation of the J/ψ mesons is assumed to be zero. The J/ψ mesons are reconstructed via the $\mu^+\mu^-$ final state. The signal yield is determined by performing an extended unbinned maximum likelihood fit to the two-dimensional $(M(\mu_1^+\mu_1^-), M(\mu_2^+\mu_2^-))$ mass distribution.

The J/ψ pair production cross section where both J/ψ mesons are in the region specified above is determined to be

$$\sigma(J/\psi J/\psi) = 13.5 \pm 0.9\,(\text{stat.}) \pm 0.8\,(\text{syst.})\ \mu\text{b}\,, \tag{8}$$

assuming negligible polarisation of the J/ψ mesons.

The LHCb results on J/ψ pair production have been compared with a data-driven prediction for the double parton scattering (DPS) mechanism and calculations performed within the single parton scattering SPS mechanism. The DPS process is of great importance since it can provide information on the transverse momenta of the partons and their correlations inside the proton, and can help in understanding various backgrounds, *e.g.* $Z + b\bar{b}$, $W^+ + W^-$, multi-jets, *etc.*, in searches for new physics. The contribution from the SPS mechanism is calculated using several approaches: leading-order colour-singlet (LO CS) and colour-octet (LO CO) calculations; the approach based on the k_{T}-factorisation method with the leading-order colour-singlet matrix element (LO k_{T}); the state-of-art incomplete (no-loops) next-to-leading-order colour-singlet (NLO* CS) calculations.

Figure 6 shows the comparisons between measurements and theoretical predictions for the differential cross sections as a function of $p_{\mathrm{T}}(J/\psi\, J/\psi)$ (left) and $y(J/\psi\, J/\psi)$ (right). In addition, series of comparisons have been computed, which can be found in [13]. Neither the DPS nor any of the SPS models describe the differential shapes. However, a fit to the differential cross sections using DPS and SPS models indicates a significant DPS contribution.

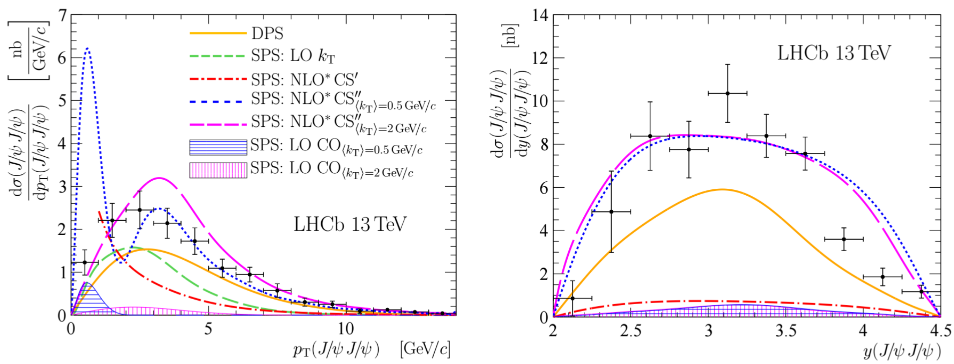

Fig. 6. The differential cross sections as a function of $p_{\mathrm{T}}(J/\psi\, J/\psi)$ and $y(J/\psi\, J/\psi)$ compared with theoretical predictions. The (black) points with error bars represent the measurements (from [13]).

4.3. Central exclusive J/ψ and $\psi(2S)$ production

Central exclusive production (CEP) leads to a unique signature with a small number of particles in the detector, either produced directly or as decay products, and two rapidity gaps that extend to the outgoing protons. A measurement made at the LHCb of the central exclusive production of J/ψ and $\psi(2S)$ mesons have been performed based on data collected in 2015 [14]. CEP charmonia candidates are selected through their characteristic signature, which is only the charmonium meson that is reconstructed from its decay to two muons. The addition of HeRSCheL subsystem extends the pseudorapidity region in which charged particles can be vetoed and roughly halves the inelastic background contribution compared to the previous LHCb measurement at lower energies.

The largest background is due to inelastic production of J/ψ and $\psi(2S)$ mesons with additional gluon radiation or proton dissociation where the additional particles are not detected at the LHCb. Since the inelastic background has a higher p_{T} than the signal, the background contribution is determined by a fit to the p_{T}^2 distribution of the meson.

The measured differential cross sections for J/ψ and $\psi(2S)$ mesons as functions of the rapidity of the mesons are shown in Fig. 7. Both measurements are better described by NLO than by LO predictions.

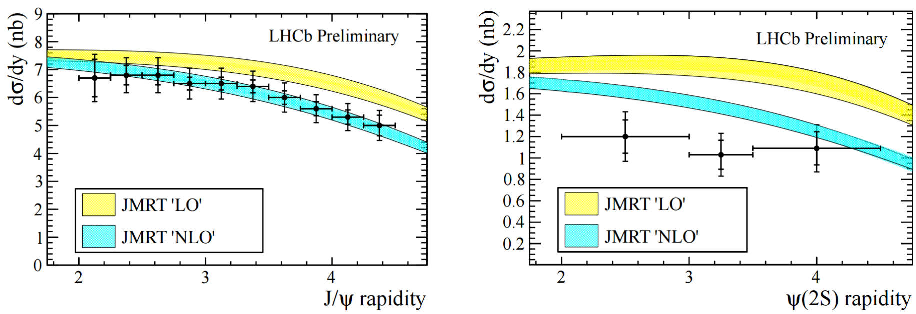

Fig. 7. Differential cross section for central exclusive J/ψ (left) and $\psi(2S)$ (right) production compared to LO and NLO predictions (from [14]).

Figure 8 shows the photoproduction cross sections for J/ψ and $\psi(2S)$ including a comparison to previous LHCb results $\sqrt{s} = 7$ TeV and to HERA data at the lower centre-of-mass energy of the photon–proton system values. Figure 8 contains also the power-law fit to H1 data hence it can be seen that this is insufficient to describe the data at the highest energies. However, the data are in a good agreement with the JMRT 'NLO' prediction. A good agreement is found between the LHCb data and an extrapolation of the H1 results for $\psi(2S)$.

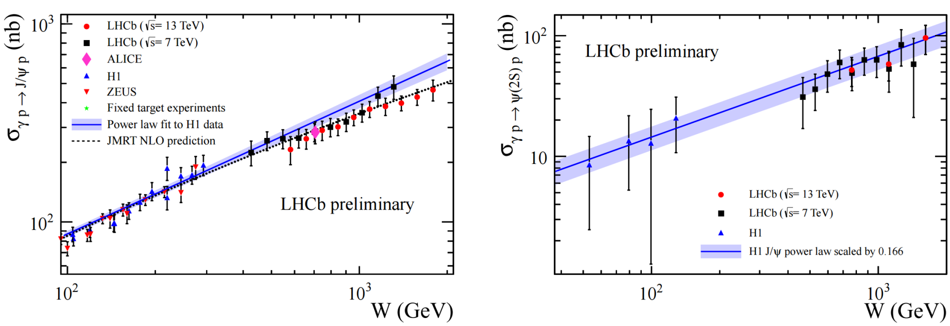

Fig. 8. Compilation of photoproduction cross-section results for various experiments for J/ψ (left) and $\psi(2S)$ (right) data (from [14]).

5. The forward Z-boson production

The inclusive Z boson production cross-section measurements have been performed at the LHCb for decays to a dimuon and dielectron final states [15]. The two final states offer statistically independent samples with largely independent systematic uncertainties.

For the dilepton invariant mass in the range of $60 < m(ll) < 120$ GeV, and where the leptons have $p_{\mathrm{T}} > 20$ GeV and $2.0 < \eta < 4.5$, is measured to be:

$$\sigma^{\mu\mu}(Z) = 198.0 \pm 0.9\ (\mathrm{stat.}) \pm 4.7\ (\mathrm{syst.}) \pm 7.7\ (\mathrm{lumi.})\ \mu\mathrm{b}\,, \tag{9}$$

$$\sigma^{ee}(Z) = 190.2 \pm 1.7\ (\mathrm{stat.}) \pm 4.7\ (\mathrm{syst.}) \pm 7.4\ (\mathrm{lumi.})\ \mu\mathrm{b}\,, \tag{10}$$

where the third uncertainty is due to the accuracy of the luminosity determination.

Figure 9 shows the integrated cross section in the fiducial acceptance and the differential measurement as a function of the Z-boson rapidity. The measured quantities are compared to the fixed-order predictions for both dimuon and dielectron final states. It may be seen in the plot that the fixed-order predictions describe the LHCb data well for a range of PDF sets. The measured differential cross section is slightly larger from the NLO pQCD predictions at lower rapidity range.

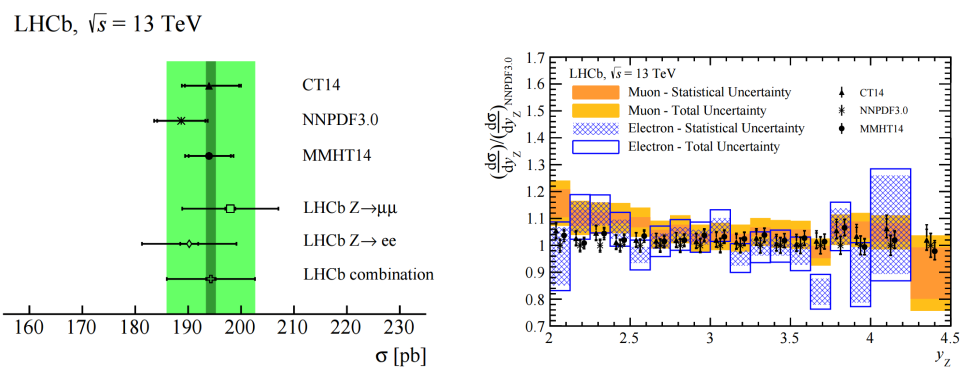

Fig. 9. The fiducial cross section compared between theory and data. In the left plot, the bands correspond to the average of the dimuon and dielectron final states, with the inner band corresponding to the statistical uncertainty and the outer band corresponding to the total uncertainty. In the right plot, the differential cross section as a function of the Z-boson rapidity is shown as ratios to the central values of the NNPDF3.0 predictions.

6. Summary and prospects

Differential cross-section measurements based on Run 2 datasets and ratios of cross sections at different centre-of-mass energies have been presented for heavy flavour (charm and beauty), quarkonia (J/ψ, J/ψ pairs and CEP J/ψ and $\psi(2S)$) and Z-boson production.

In general, the differential cross sections are described by the predictions within uncertainties.

Measurements of differential cross sections for CEP J/ψ and $\psi(2S)$ have been presented. A new instrumentation of the LHCb detector with forward shower counters significantly improved the background evaluation for this kind of analyses. The presented results agree with the shapes predicted by NLO calculations. The 13 TeV data extends the W span to almost 2 TeV in the power-law trend. It was shown that the power-law fit to H1 data is insufficient to describe the LHCb data.

This research was supported in part by the National Research Centre, Poland (NCN), grant No. UMO-2015/18/M/ST2/00123 and the Ministry of Science and Higher Education, Poland.

REFERENCES

[1] A.A. Alves, Jr. *et al.* [LHCb Collaboration], *JINST* **3**, S08005 (2008).
[2] `http://lhcb-operationsplots.web.cern.ch`
[3] O. Zenaiev *et al.* [PROSA Collaboration], *Eur. Phys. J. C* **75**, 396 (2015) [`arXiv:1503.04581 [hep-ph]`].
[4] R. Aaij *et al.* [LHCb Collaboration], *J. High Energy Phys.* **1603**, 159 (2016) [*Erratum ibid.* **1609**, 013 (2016)] [`arXiv:1510.01707 [hep-ex]`].
[5] R. Aaij *et al.* [LHCb Collaboration], `arXiv:1610.02230 [hep-ex]`.
[6] R. Aaij *et al.* [LHCb Collaboration], *Nucl. Phys. B* **871**, 1 (2013) [`arXiv:1302.2864 [hep-ex]`].
[7] B.A. Kniehl, G. Kramer, I. Schienbein, H. Spiesberger, *Phys. Rev. D* **79**, 094009 (2009) [`arXiv:0901.4130 [hep-ph]`].
[8] M. Cacciari *et al.*, *J. High Energy Phys.* **1210**, 137 (2012) [`arXiv:1205.6344 [hep-ph]`].
[9] R. Aaij *et al.* [LHCb Collaboration], *Phys. Rev. Lett.* **118**, 052002 (2017) [`arXiv:1612.05140 [hep-ex]`].
[10] R. Aaij *et al.*, *JINST* **8**, P04022 (2013) [`arXiv:1211.3055 [hep-ex]`].
[11] R. Aaij *et al.* [LHCb Collaboration], *J. High Energy Phys.* **1510**, 172 (2015) [`arXiv:1509.00771 [hep-ex]`].
[12] P.L. Cho, A.K. Leibovich, *Phys. Rev. D* **53**, 6203 (1996) [`arXiv:hep-ph/9511315`].
[13] R. Aaij *et al.* [LHCb Collaboration], `arXiv:1612.07451 [hep-ex]`.
[14] LHCb Collaboration, LHCb-CONF-2016-007, CERN-LHCb-CONF-2016-007.
[15] R. Aaij *et al.* [LHCb Collaboration], *J. High Energy Phys.* **1609**, 136 (2016) [`arXiv:1607.06495 [hep-ex]`].